

Shape Sensing and Damage Detection of Thin-Walled Cylinders Using an Inverse Finite Element Method

Ionel D. Craiu, Mihai Nedelcu

Abstract—Thin-walled cylinders are often used by the offshore industry as columns of floating installations. Based on observed strains, the inverse Finite Element Method (iFEM) may rebuild the deformation of structures. Structural Health Monitoring uses this approach extensively. However, the number of in-situ strain gauges is what determines how accurate it is, and for shell structures with complicated deformation, this number can easily become too high for practical use. Any thin-walled beam member's complicated deformation can be modeled by the Generalized Beam Theory (GBT) as a linear combination of pre-specified cross-section deformation modes. GBT uses bar finite elements as opposed to shell finite elements. This paper proposes an iFEM/GBT formulation for the shape sensing of thin-walled cylinders based on these benefits. This method significantly reduces the number of strain gauges compared to using the traditional inverse-shell finite elements. Using numerical simulations, dent damage detection is achieved by comparing the strain distributions of the undamaged and damaged members. The effect of noise on strain measurements is also investigated.

Keywords—Damage detection, generalized beam theory, inverse finite element method, shape sensing.

I. INTRODUCTION

SHAPE monitoring stands as a pivotal concern of Structural Health Monitoring across various domains, encompassing ocean engineering (ship and submarine hulls, floating offshore installations), civil engineering (bridges, wind turbines), and aerospace engineering (aircraft wings). This paper presents an approach for monitoring floating offshore or land-based wind turbines. The focus is on shape sensing and identifying potential damage for the thin-walled cylinders acting as columns to such structures. The study is based on the shape sensing formulation recently developed by Nedelcu [1] for thin-walled cylinders, which relies on the iFEM originally developed by Tessler and Spangler [2], [3], combined with the GBT [4]. GBT is a bar theory that has the capability to describe the complex deformation of any thin-walled beam member as a linear combination of pre-determined cross section deformation modes. iFEM can find the degrees of freedom (DOF) and consequently reconstruct the displacement/strain field, by minimizing the differences between measured and theoretical strains. The iFEM/GBT formulation significantly reduces the DOF number and as a result, the strain measurement points, as evidenced in [1]. Furthermore, Li et al. [5] developed a technique for detecting damage that takes into account the

differences between the strains reconstructed from undamaged and damaged structures. This proposed damage parameter will be employed in this study, in combination with the iFEM/GBT approach. In this study, the effects of noisy strain measurements on the accuracy of the iFEM solution, initially studied by Kefal et al. [6], is also examined, using strain measurements affected by random noise. Finally, three numerical examples are presented to validate the proposed theory. For these, the measured strains will be simulated using a shell FE analysis.

II. GENERALIZED BEAM THEORY FOR CYLINDRICAL SHELLS

Fig. 1 shows the configuration of a cylindrical element, characterized by its length (L), its radius (r) and its thickness (t). The coordinate systems include the global and local coordinate systems (X, Y, Z) and (x, θ, z) respectively. By employing Kirchhoff's thin plate assumption, the displacements of the shell are derived from the mid-surface displacements. Specifically, the meridional, circumferential and transversal displacements along the local axes are represented by u, v and w respectively.

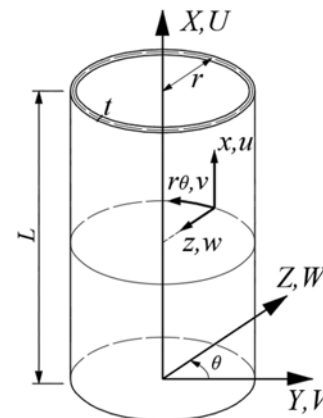


Fig. 1 The components of displacements in the local and global coordinate system

A. Linear Kinematic Relations

According to the Love-Timoshenko theory, the linear kinematic relations in the case of cylindrical shells are [1]:

I. D. Craiu and M. Nedelcu are with the Department of Structural Mechanics, Faculty of Civil Engineering, Technical University of Cluj-Napoca,

Romania (e-mail: Mihai.Nedelcu@mecon.utcluj.ro).

Ionel.Craiu@mecon.utcluj.ro,

$$\begin{aligned} \varepsilon_{xx} &= u_{,x} - z w_{,xx} \\ \varepsilon_{\theta\theta} &= \frac{v_{,\theta} - w}{r} - z \frac{v_{,\theta} + w_{,\theta\theta}}{r^2} \\ \gamma_{x\theta} &= \frac{u_{,\theta}}{r} + v_{,x} + z \frac{v_{,x} - 2w_{,x\theta}}{2r} \end{aligned} \quad (1)$$

According to GBT, the mid-surface displacements u , v and w are expressed as a linear combination of orthogonal functions as in (2), where $u_k(\theta)$, $v_k(\theta)$, $w_k(\theta)$ are the cross-section displacement functions for mode k while $\phi_k(x)$ is the corresponding modal amplitude function defined along the length [1].

$$\begin{aligned} u &= \sum_{k=1}^{n_{modes}} u_k(\theta) \phi_{k,x}(x), \\ v &= \sum_{k=1}^{n_{modes}} v_k(\theta) \phi_k(x) \\ w &= \sum_{k=1}^{n_{modes}} w_k(\theta) \phi_k(x) \end{aligned} \quad (2)$$

B. Shell-Type Deformation Modes

The conventional GBT commonly supposes that membrane shear strains ($\gamma_{x\theta}^M$), and transverse strains ($\varepsilon_{\theta\theta}^M$) have negligible effect, as mentioned in [7]. Thus, considering them null and using (1), the displacement components of the cross-section, $v_k(\theta)$ and $w_k(\theta)$ can be obtained based on the warping component, $u_k(\theta)$.

$$v_k = -\frac{u_{k,\theta}}{r}; \quad w_k = v_{k,\theta} = -\frac{u_{k,\theta\theta}}{r} \quad (3)$$

In the case of circular closed cross-sections, two independent sets of trigonometric functions, which are given in (4), have been widely used in previous research papers [1], [7]. There, n represents the number of shell modes that are considered.

$$u_k = \begin{cases} r \sin(m\theta), m = \frac{k+1}{2}, k = 1, 3, 5, \dots, n-1 \\ r \cos(m\theta), m = \frac{k}{2}, k = 2, 4, 6, \dots, n \end{cases} \quad (4)$$

Fig. 2 shows the in-plane shapes of the first 12 shell-type deformation modes.

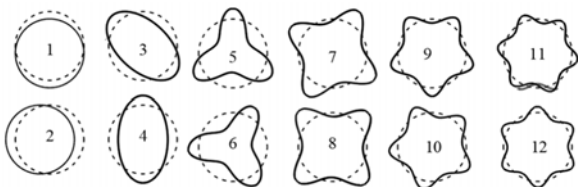


Fig. 2 The shell-type deformation modes (in-plane shapes)

C. Shear Deformation Modes

During the previous research [1], [7], it was found that Vlasov's hypothesis ($\gamma_{x\theta}^M = 0$) has certain limitations that can lead to significant errors because the shell-type deformation modes are not capable to capture the membrane shear effect on the member deformation (especially for short members). For

this reason, Nedelcu [1] considered the next shear modes, which will be adopted here as well:

- "Shear v-w" modes: $u_k = 0$; v_k and w_k remain as described for shell-type modes (see (3) and (4)).

D. Additional Deformation Modes

Due to the assumptions used ($\gamma_{x\theta}^M = 0$ and $\varepsilon_{\theta\theta}^M = 0$), the previously presented deformation modes cannot represent three fundamental deformation types and for this reason, the following additional deformation modes are introduced [1]-[7]:

- Axial extension mode: $u_e = 1, v_e = 0, w_e = 0$;
- Axisymmetric extension mode: $u_a = 0, v_a = 0, w_a = 1$;
- Torsion mode: $u_t = 0, v_t = r, w_t = 0$.

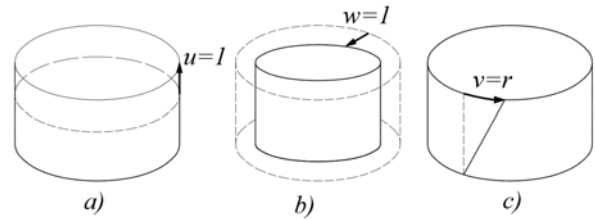


Fig. 3 The additional modes: (a) axial extension, (b) axisymmetric extension, (c) torsion

E. GBT Finite Element Formulation

To find the displacement field, it is necessary to use amplitude functions, defined as $\phi_k(x)$, associated with the deformation modes of the known cross section. To approximate these amplitude functions, Nedelcu [1] used the polynomial shape functions proposed by Silvestre and Camotim [8] and Basaglia et al. [9] involving Lagrange and Hermite cubic polynomial primitives. These shape functions were successfully adopted in this paper as well.

By incorporating the shape functions in the kinematic relations given in (1), the relations between the strain components and the DOF vector (q_e) at the FE level, are found as in (5):

$$\begin{Bmatrix} \varepsilon_{xx} \\ \varepsilon_{\theta\theta} \\ \gamma_{x\theta} \end{Bmatrix} = \begin{Bmatrix} B_{xx} \\ B_{\theta\theta} \\ B_{x\theta} \end{Bmatrix} q^e \quad (5)$$

where B_{xx} , $B_{\theta\theta}$, $B_{x\theta}$ are the "strain-DOF" matrices.

III. iFEM/GBT FORMULATION

The determination of DOF in iFEM involves the minimization of differences between theoretical strains $e(q) = \{\varepsilon_{xx}, \varepsilon_{\theta\theta}, \gamma_{x\theta}\}^T$ and the measured strains e^e . This optimization is realized through the minimization of a weighted least-squares functional Φ with respect to the nodal DOF.

$$\Phi(q) = \|e(q) - e^e\|^2 \quad (6)$$

The thin-walled cylinder is discretized into longitudinal 1D inverse finite elements. For each finite element, a distinct functional $\Phi_e(q_e)$ is formulated in the following manner:

$$\Phi_e(\mathbf{q}^e) = \frac{L_e}{n_e} \sum_{i=1}^{n_e} \left\{ \omega_{xx} [\varepsilon_{xx}(\mathbf{q}^e)_{(i)} - \varepsilon_{xx}^e]_{(i)}^2 + \omega_{\theta\theta} [\varepsilon_{\theta\theta}(\mathbf{q}^e)_{(i)} - \varepsilon_{\theta\theta}^e]_{(i)}^2 + \omega_{x\theta} [\gamma_{x\theta}(\mathbf{q}^e)_{(i)} - \gamma_{x\theta}^e]_{(i)}^2 \right\} \quad (7)$$

In (7), n_e is the number of strain points within the FE and ω_{xx} , $\omega_{\theta\theta}$ and $\omega_{x\theta}$ are the weighting coefficients associated with the strain components (in this study, they are all equal to 1).

The least squares functional is minimized with respect to the DOF, resulting in the following expression (where \mathbf{k}^e is the coefficient matrix and \mathbf{f}^e is the constant terms vector depending on the measured strains):

$$\mathbf{k}^e \mathbf{q}^e = \mathbf{f}^e \quad (8)$$

$$\mathbf{k}^e = \sum_{i=1}^{n_e} [B_{xx(i)} B_{xx(i)}^T + B_{\theta\theta(i)} B_{\theta\theta(i)}^T + B_{x\theta(i)} B_{x\theta(i)}^T] \quad (9)$$

$$\mathbf{f}^e = \sum_{i=1}^{n_e} [\varepsilon_{xx}^e B_{xx(i)}^T + \varepsilon_{\theta\theta}^e B_{\theta\theta(i)}^T + \gamma_{x\theta}^e B_{x\theta(i)}^T] \quad (10)$$

The comprehensive set of equations, $\mathbf{K}\mathbf{q} = \mathbf{F}$, is subsequently constructed for the entire model. Here, \mathbf{K} is a non-singular matrix that remains constant for a given distribution of FEs and strain points. The \mathbf{F} vector is dependent on the measured strains and needs to be updated for each new measurement.

IV. GBT MODAL IDENTIFICATION

The modal identification, developed for the first time by Nedelcu [1] for cylindrical members, has the role of identifying the deformation modes with a substantial influence on the behavior of the element, under different loads and support. This method is based on the orthogonality properties of the deformation modes (for example, $\oint u_k u_i d\theta = 0$, for any $k \neq i$).

A large number of deformation modes are initially proposed, after which the integral of the product of the cross-section displacement functions is calculated for each shell-type and additional mode as follows:

$$I_u = \oint u_k u_k d\theta, I_v = \oint v_k v_k d\theta, I_w = \oint w_k w_k d\theta \quad (11)$$

Next, an FE shell model is performed and after the analysis, the displacement field is extracted in the global coordinate system (U_{FE} , V_{FE} , W_{FE}). This is later transformed into the local coordinate system resulting in $u_{FE}(\theta, x)$, $v_{FE}(\theta, x)$, $w_{FE}(\theta, x)$.

Numerical integration is then performed to find the amplitude modal functions $\phi(x)$ and their derivatives $\phi_{k,x}(x)$ in any cross-section j , as in (12):

$$\begin{aligned} \phi_{k,x}(x_j) &= \frac{\oint u_k(\theta) u_{FE}(\theta, x_j) d\theta}{I_u} \\ \phi_k(x_j) &= \frac{\oint v_k(\theta) v_{FE}(\theta, x_j) d\theta}{I_v} \\ \phi_k(x_j) &= \frac{\oint w_k(\theta) w_{FE}(\theta, x_j) d\theta}{I_w} \end{aligned} \quad (12)$$

V. OPTIMIZING THE SENSOR/FE CONFIGURATION

The optimization process for determining the number and

positions of sensor points, corroborated with the configuration of the 1D finite element (FE) mesh, can be strategically improved according to the following steps:

1. An analysis utilizing shell-type finite elements is realized to extract strain and displacement fields;
2. Modal identification is executed based on the displacement field, leading to the discovery of significant GBT deformation modes;
3. An initial configuration of sensor points and a 1D FE mesh is proposed;
4. Simulated measured strains \mathbf{e}_e are extracted in the sensor locations;
5. The iFEM/GBT analysis employs the relevant GBT deformation modes and the simulated measured strains \mathbf{e}_e to reconstruct the displacement field (\mathbf{U}_{inv}).
6. A comparison is made between the reconstructed displacements (\mathbf{U}_{inv}) and the displacements obtained from the FE shell analysis (\mathbf{U}_{FE}) using the total displacements $U_t = \sqrt{U^2 + V^2 + W^2}$;
7. The error indicator is the maximum relative error. If this indicator falls below a predetermined tolerance, the final sensor configuration is considered optimal. If the error indicator exceeds the tolerance, a new sensor/FE configuration is proposed, and the analysis recommences from step 4.

VI. DAMAGE DETECTION

The primary aim of this paper is to identify potential areas of damage within the analyzed cylindrical structure. This damage detection process involves a comparison between the distributions of von Mises strains in the undamaged state ($\varepsilon_{undamaged}$) and the damaged state ($\varepsilon_{damaged}$) of the member. The evaluation of damage is quantified using the parameter D , introduced by Li et al. [5], which is computed as in (13). There, μ is Poisson's ratio.

$$D = \left[\frac{\varepsilon_{damaged} - \varepsilon_{undamaged}}{\varepsilon_{undamaged}} \right] \quad (13)$$

$$\varepsilon = \frac{\sqrt{(\varepsilon_{xx} - \varepsilon_{\theta\theta})^2 + (\varepsilon_{xx} - \varepsilon_{zz})^2 + (\varepsilon_{\theta\theta} - \varepsilon_{zz})^2 + 6\gamma_{x\theta}^2}}{\sqrt{2}} \quad (14)$$

$$\varepsilon_{zz} = \frac{\mu}{\mu - 1} (\varepsilon_{xx} + \varepsilon_{\theta\theta}) \quad (15)$$

VII. THE EFFECTS OF NOISY STRAIN MEASUREMENTS ON THE ACCURACY OF THE IFEM SOLUTION

An important aspect that should not be overlooked in the case of measurements with strain rosettes, is the influence of noise that can appear in the circuits and can disturb the desired signal.

Kefal et al. [6] took into account the influence of noise on the measurements, using the SNR parameter. SNR (Signal-to-Noise Ratio) represents the ratio between the power of the desired signal and the power of the background noise in measurement. Essentially, SNR characterizes how clear or distinct the signal is in comparison to the level of noise present. A higher SNR value indicates that the signal is stronger compared to the noise. A lower SNR value indicates that the

signal is less dominant compared to the noise.

$$SNR_{db} = 10 \log_{10} \frac{P_{signal}}{P_{noise}} \quad (16)$$

where P_{signal} and P_{noise} are respectively the average power of the signal and noise [6].

In this paper, the influence of noise on measurements was studied for two SNR values (13.01 db and 6.91db), as described in the next chapter. The presence of noise in the measurements was simulated by introducing white Gaussian noise, using the "awgn" function in MATLAB [11]. White Gaussian noise is a type of random signal with zero mean and following a Gaussian (normal) probability distribution.

VIII. NUMERICAL EXAMPLES

To validate the proposed theory, three numerical examples were made, using Abaqus [10] and MATLAB [11]. These include the same geometry for the cylinder ($L = 300$ mm, $r = 50$ mm and $t = 1$ mm) and the same material properties (Young's modulus $E = 210$ GPa and Poisson ratio $\mu = 0.3$). All three elements are fixed at one end and free at the opposite end. Each example has different loading conditions, as will be presented later.

The main objective was damage detection, using the parameter D , described in Chapter IV. Moreover, the influence of noise on the measurements was included, both for shape sensing and damage detection.

The next three steps were followed for all numerical examples:

- 1) For each example, modeling was performed in Abaqus [10], using shell S4R linear quadrilateral finite elements. There are 60 nodes on cross-section and 64 on the meridian. The damage is induced in the FE shell model at different positions by reducing Young's modulus in the damaged region. This region covers a very small area given by four connected shell FEs. There are two cases of damage, first a major reduction ($E = 0.21$ MPa) and then a minor reduction ($E = 190\ 000$ MPa).
- 2) After analysis, the simulated strains are extracted at the

positions of the fictitious strain sensors. To take into account the effect of noise, white Gaussian noise was introduced over these "measurements" using the SNR parameter described in (16). Using (16), the SNR values corresponding to 5% noise and 15% noise, can be calculated as 13.01 dB and 6.91 dB respectively, as in (17) and (18):

$$SNR_{db} = 10 \log_{10} \frac{0.85}{0.15} = 6.91 \text{ db} \quad (17)$$

$$SNR_{db} = 10 \log_{10} \frac{0.95}{0.05} = 13.01 \text{ db} \quad (18)$$

- 3) The iFEM/GBT formulation, modal identification and damage detection procedure are implemented using a MATLAB application [11]. A tolerance value of 1% for maximum relative error was chosen for modal identification. The sensor/FE configuration was optimized using a tolerance value of 5%.

The proposed number of strain rosettes for which the deformed shape was successfully reconstructed is shown for each case. The agreement between the total shell FE displacements and the reconstructed displacements, both in the presence of noise and without noise, are highlighted. Subsequently, the damage parameter D is presented on the entire surface using the strains reconstructed based on the iFEM/GBT methods, with and without noise.

B. Member under Uniformly Distributed Axial Load

Resultant of the distributed load, $P = 50$ kN; number of sensors = 40.

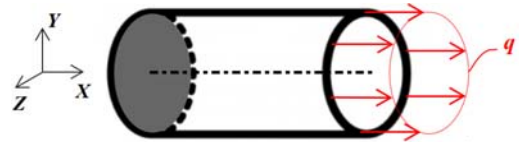


Fig. 4 Member under uniformly distributed axial load

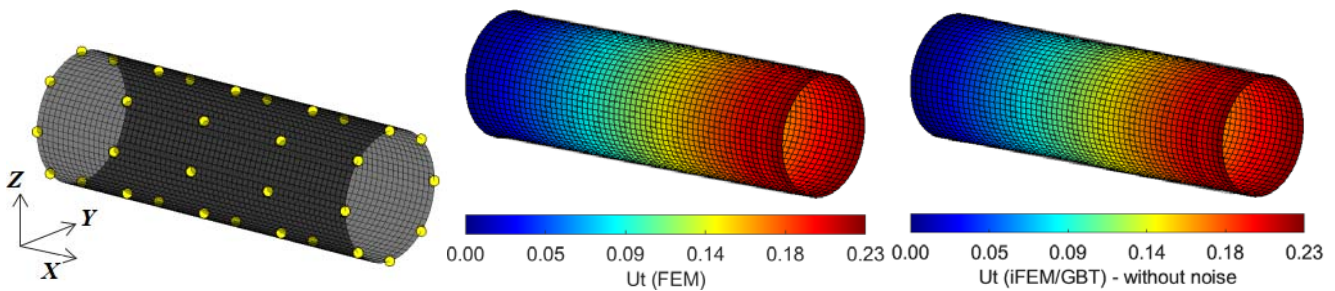


Fig. 5 Sensor configuration and contour plots of U_t displacements (FEM vs. iFEM/GBT) - without noise

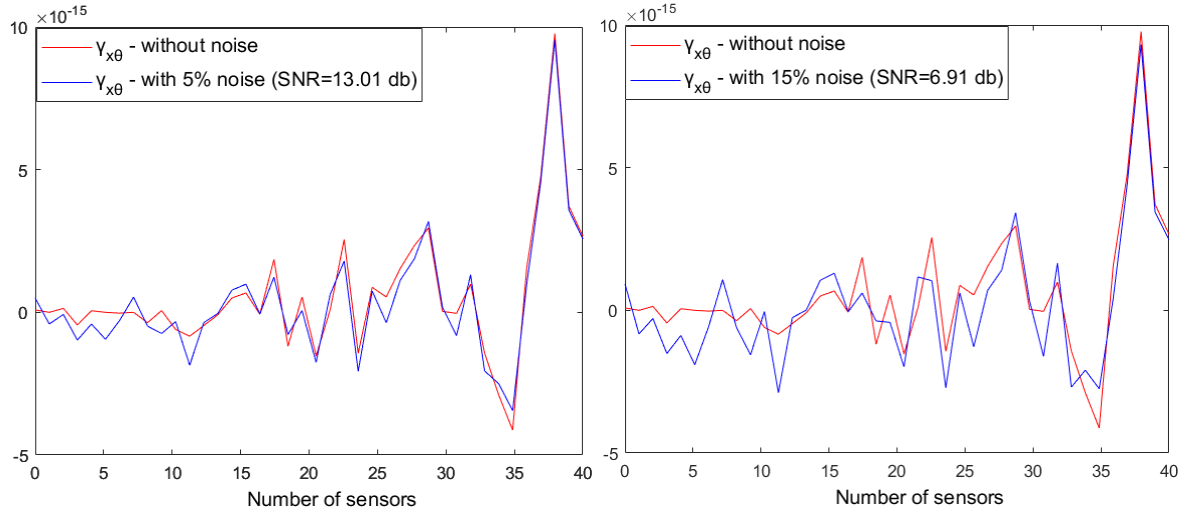


Fig. 6 Comparison of the strain measurements (γ_{x0}) with 0%, 5% and 15% noise

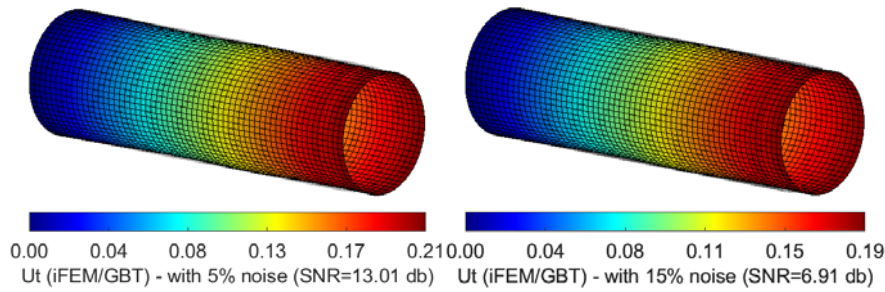


Fig. 7 Contour plots of U_t displacements (iFEM/GBT) - with 5% and 15% noise

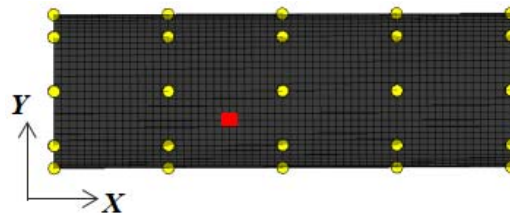


Fig. 8 Proposed damaged location

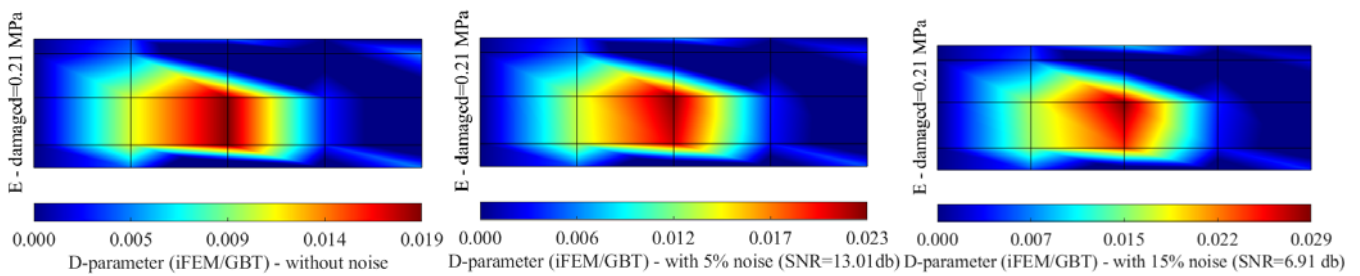


Fig. 9 Damage detection (iFEM/GBT) - with 0%, 5% and 15% noise ($E_{\text{damaged}} = 0.21 \text{ MPa}$)

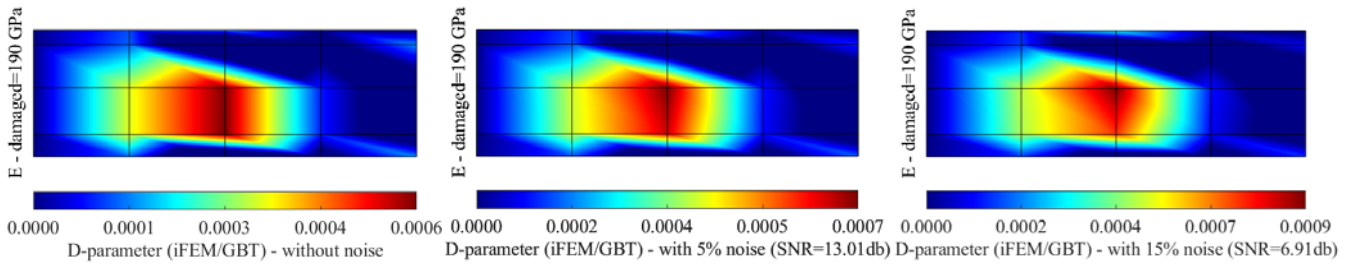


Fig. 10 Damage detection (iFEM/GBT) - with 0%, 5% and 15% noise (E-damaged = 190 GPa)

B. Member under Uniformly Distributed Transverse Load

Load: $q = 4 \text{ kN/m}$; because of the symmetry plane of this structure (Oxy), it is possible to conduct iFEM/GBT analysis on only one half of the cylinder. Thus, 35 sensors (for shape sensing) and 77 sensors (for damage detection) were placed on half of the geometry.

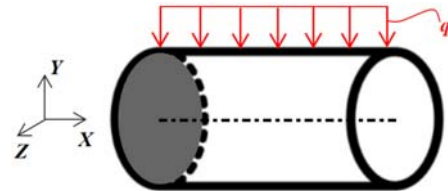


Fig. 11 Member under uniformly distributed transverse load

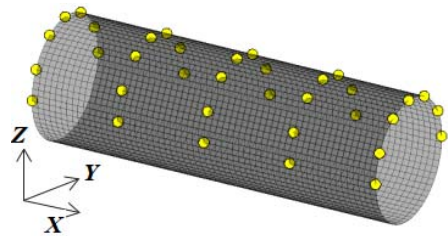


Fig. 12 Sensor configuration for shape sensing

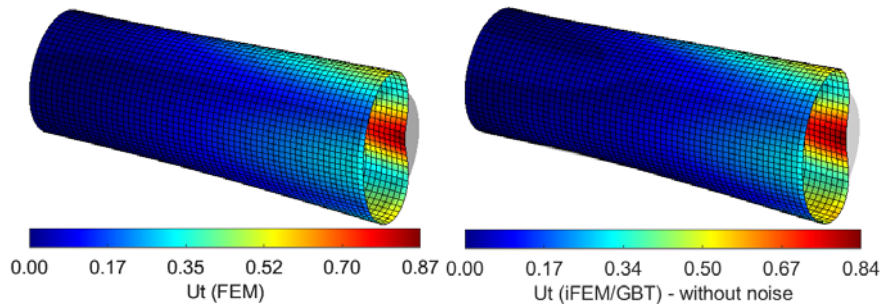


Fig. 13 Contour plots of U_t displacements (FEM vs. iFEM/GBT) - without noise

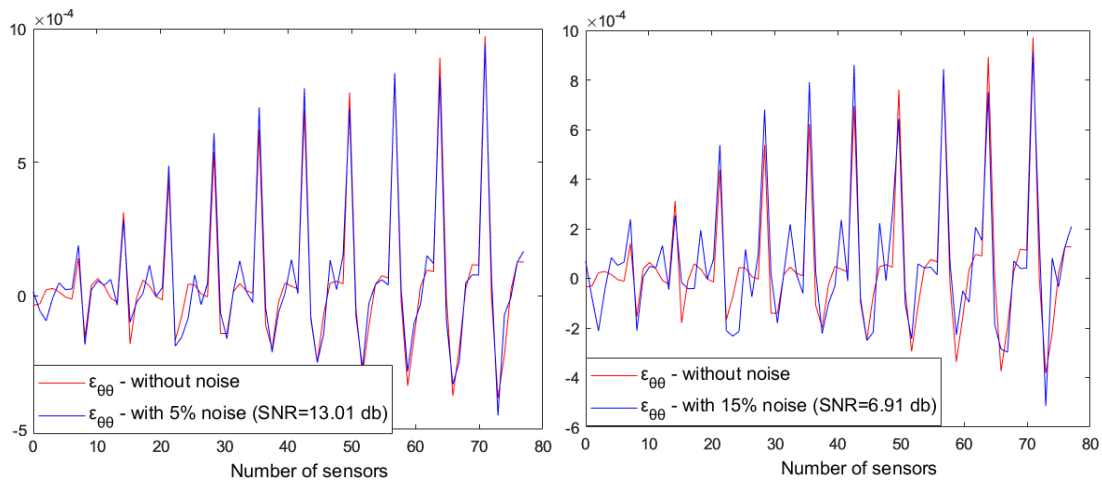


Fig. 14 Comparison of the strain measurements ($\epsilon_{\theta\theta}$) with 0%, 5% and 15% noise

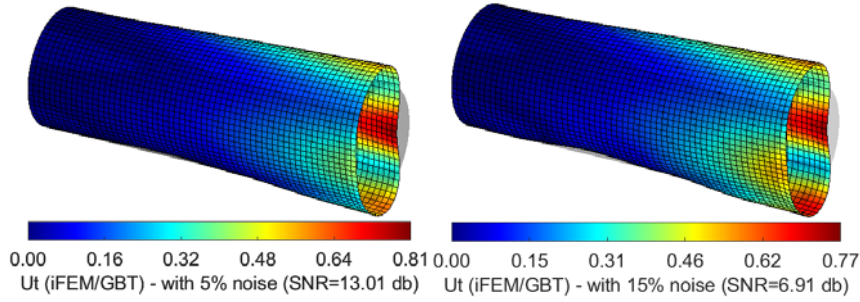


Fig. 15 Contour plots of U_t displacements (iFEM/GBT) - with 5% and 15% noise

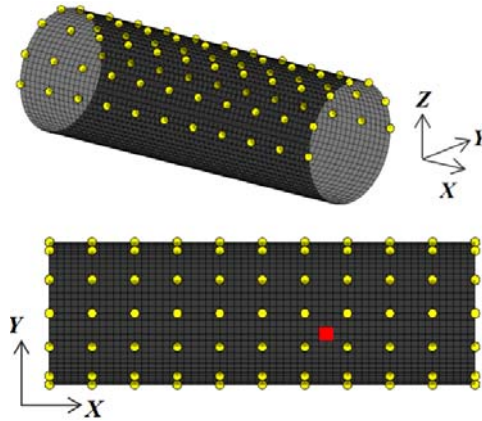


Fig. 16 Sensor configuration and proposed location for damage detection

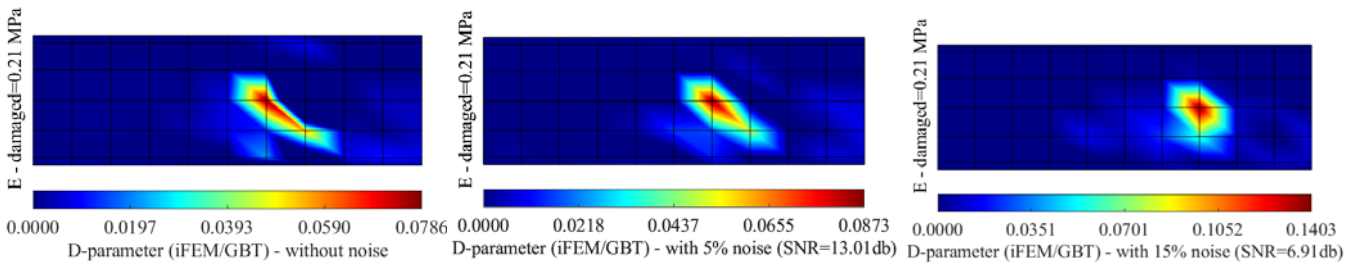


Fig. 17 Damage detection (iFEM/GBT) - with 0%, 5% and 15% noise ($E_{\text{damaged}} = 0.21 \text{ MPa}$)

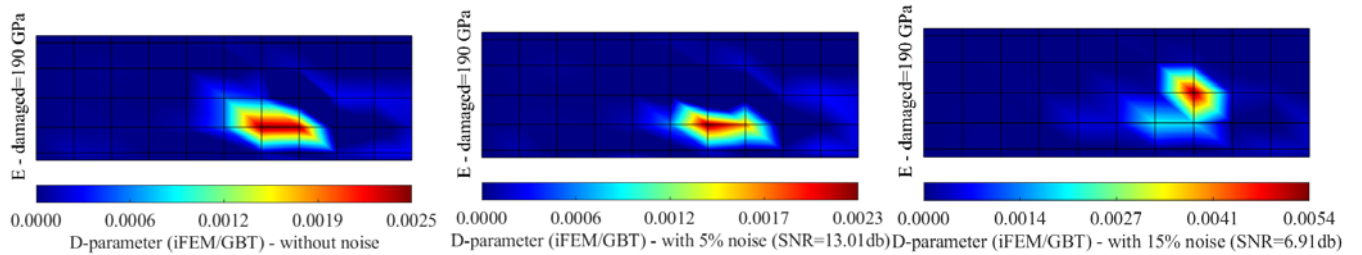


Fig. 18 Damage detection (iFEM/GBT) - with 0%, 5% and 15% noise ($E_{\text{damaged}} = 190 \text{ GPa}$)

C. Member under End Loads

F - loads: $F_x = -0.5 \text{ kN}$; $F_y = 0.5 \text{ kN}$; $F_z = 1 \text{ kN}$; M - loads:
 $M_x = -0.5 \text{ kNm}$; $M_y = 1 \text{ kNm}$; $M_z = 0.5 \text{ kNm}$; Number of
 sensors = 56.

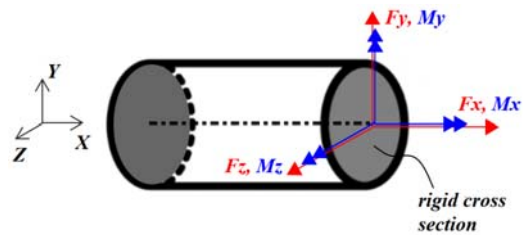


Fig. 19 Member under end loads

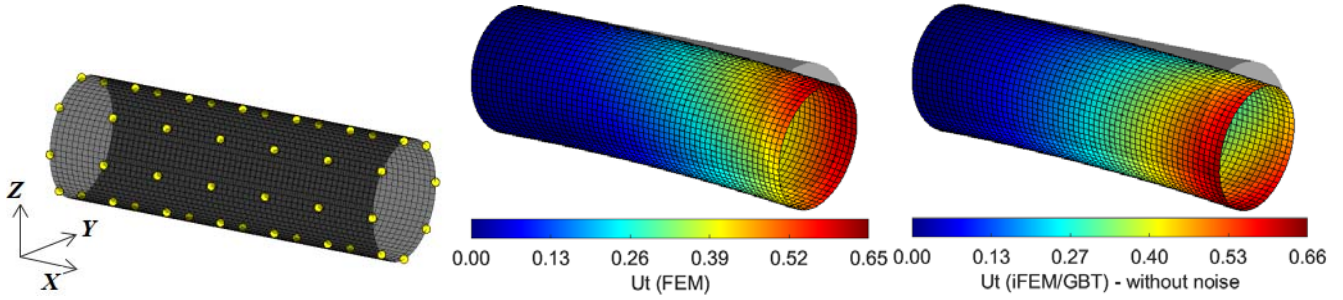


Fig. 20 Sensor configuration and contour plots of U_t displacements (FEM vs. iFEM/GBT) - without noise

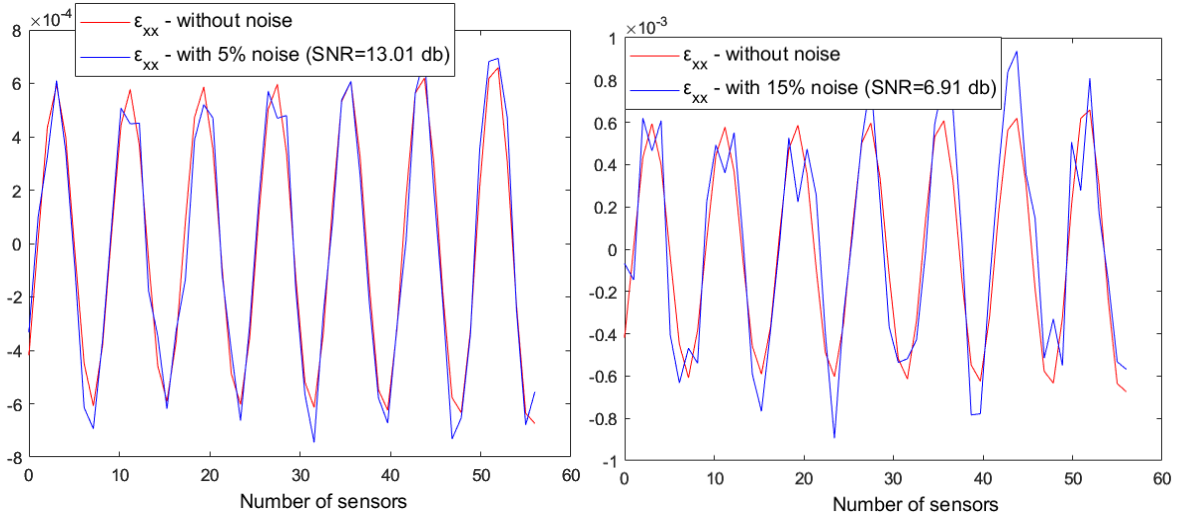


Fig. 21 Comparison of the strain measurements (ϵ_{xx}) with 0%, 5% and 15% noise

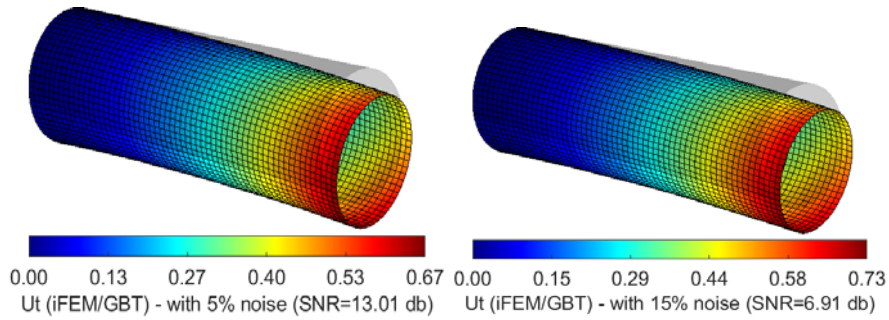


Fig. 22 Contour plots of U_t displacements (iFEM/GBT) - with 5% and 15% noise

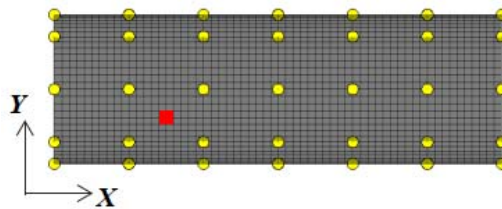


Fig. 23 Proposed damaged location

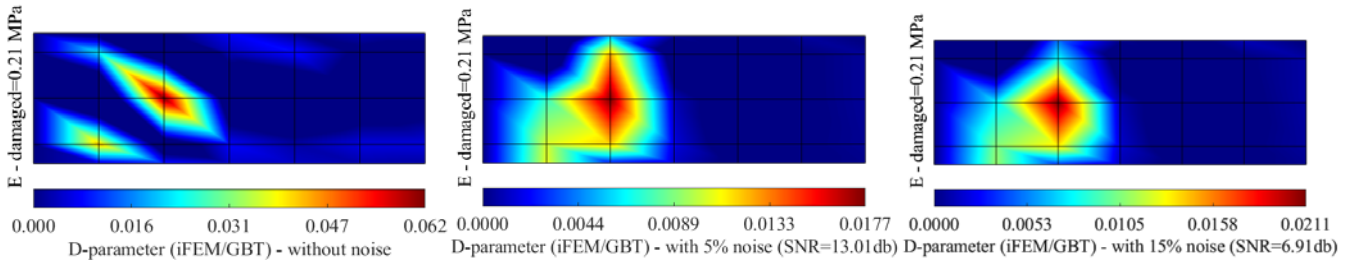


Fig. 24 Damage detection (iFEM/GBT) - with 0%, 5% and 15% noise (E-damaged = 0.21 MPa)

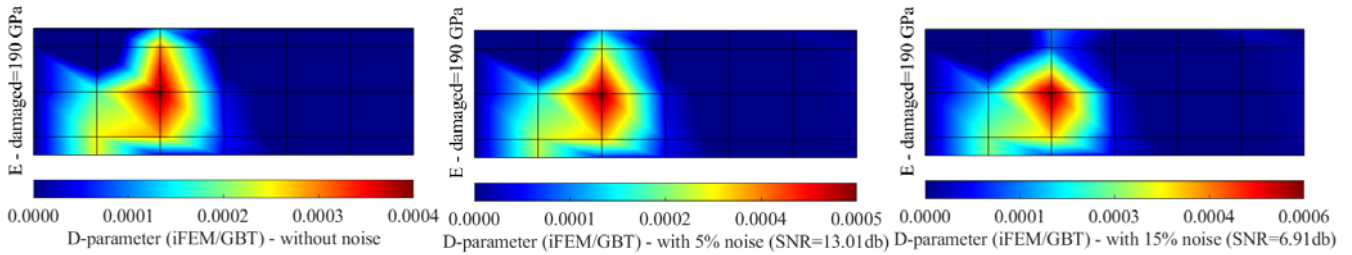


Fig. 25 Damage detection (iFEM/GBT) - with 0%, 5% and 15% noise (E-damaged = 190 GPa)

IX. CONCLUSIONS

Analyzing the obtained results, we can see that the proposed iFEM/GBT method, together with the damage parameter D , offers satisfactory results in terms of detecting potential damage that can occur to a cylindrical element. For the case of uniformly distributed axial load and the case of loads concentrated at the end, the number of sensors required for damage detection is the same as that required for shape sensing (40 and 56, respectively). For the case of uniformly distributed transverse load, an increase in the number of sensors is required for the proper detection of damage: from 35 (for shape sensing) to 77. It should be noted that for all cases, a very small damaged area (approximately 2 cm^2) was well detected. Also, the damage was correctly detected both for a drastic reduction of Young's modulus ($E = 0.21 \text{ MPa}$) and for a small reduction ($E = 190,000 \text{ MPa}$).

Another important aspect that was analyzed refers to the influence of noise on the measurement signal. The SNR values of 6.91 db and 13.01 db were entered into the analysis, which represents a noise contribution of 15% and 5% respectively, relative to the unaffected signal. Through the illustrations representing the variation of the strains with and without noise, it can be seen that the noise influences the measurements, especially for a low SNR (6.91 db). But even so, the desired results are still obtained. The differences are small between the element analyzed without noise and the element analyzed in the presence of noise, both for shape sensing and damage detection. The best results were obtained with an SNR of 13.01 db, which was expected, and it can be said that this SNR value is a good estimate of the real noise level.

REFERENCES

[1] M. Nedelcu, *Optimisation of inverse Finite Element Method for shape sensing of thin-walled cylinders by using Generalised Beam Theory*, Thin-Walled Structures, 188, 110865, 2023;
 [2] A. Tessler, J.L. Spangler, *A variational principle for reconstruction of*

elastic deformation of shear deformable plates and shells, NASA TM-2003-212445, 2003;
 [3] A. Tessler, J.L. Spangler, *A least-squares variational method for full-field reconstruction of elastic deformations in shear-deformable plates and shells*, Comput. Methods Appl. Mech. Eng. 194 (2), 327–339, 2005;
 [4] R. Schardt, *Verallgemeinerte Technische Biegetheorie*, Springer Verlag, Berlin, 1989 (in German);
 [5] M. Li, A. Kefal, B.C. Cerik, E. Oterkus, *Dent damage identification in stiffened cylindrical structures using inverse Finite Element Method*. Ocean Eng 198, 106944, 2020;
 [6] A. Kefal, E. Oterkus, A. Tessler, J.L. Spangler, *A quadrilateral inverse-shell element with drilling degrees of freedom for shape sensing and structural health monitoring*, Engineering Science and Technology an International Journal, vol. 19, Issue 3, September 2016, Pages 1299-1313;
 [7] N. Silvestre, *Generalised beam theory to analyse the buckling behaviour of circular cylindrical shells and tubes*, Thin-Walled Structures, 45 (2), 185–198, 2007;
 [8] N. Silvestre, D. Camotim, *Non-linear generalized beam theory for cold-formed steel members*. Struct. Stab. Dyn. 3 (4), 461–490, 2003;
 [9] C. Basaglia, D. Camotim, N. Silvestre, *Non-linear GBT formulation for open-section thin-walled members with arbitrary support conditions*. Comput. Struct. 89 (21–22), 1906–19, 2011;
 [10] ABAQUS Standard (Version 6.3), 2002, Hibbit Karlsson and Sorensen Inc;
 [11] MATLAB 2005. Version 7.1.0246 Documentation, The Mathwork Inc.